Indian Journal of Chemistry
Vol. 65, June 2026, pp. 594-606
DOI: 10.56042/ijc.v65i6.27116

# Multifunctional metal–dithiolate architectures: Bridging coordination chemistry, molecular memory, and anticancer potential through mixed-ligand transition metal(II) complexes

Arijit Das*[a], Syed Arshad Hussain*[b], Rahul Deb[b], Debasish Maiti*[c], Snehashish Modak[c], Debajyoti Nath[d], Abhijit Bhattacharya[a], Kartick Lal Bhowmik[a] & Paresh Debnath*[a,d]

[a] Department of Chemistry, BBM College, Agartala 799 004, West Tripura, India

[b] Thin film and Nanoscience Laboratory, Tripura University, Suryamaninagar 799 022, Tripura, India

[c] Department of Human Physiology, Tripura University, Suryamaninagar 799 022, Tripura, India

[d] Department of Education, NIT Agartala, Jirania 799 046, West Tripura, India

E-mail: arijitdas78chem@gmail.com, sahussain@tripurauniv.ac.in, debasish.maiti@tripurauniv.ac.in, pareshchem1990@gmail.com

*Received 31 December 2025; accepted (revised) 15 June 2026*

The rational design of multifunctional coordination compounds remains a key challenge at the interface of inorganic chemistry, materials science, and biomedicine. In this work, a new family of mixed-ligand M(II) complexes (M = Ni, Co, Zn, and Cd) incorporating the sulfur-rich 1-cyano-carboethoxyethylene-2,2-dithiolate ($CED^{2-}$) and the rigid nitrogen-donor ligand 4,4′-bipyridine has been synthesized and systematically investigated. The four different complexes have been characterized by CHN analysis, molar conductivity, UV-Vis, fluorescence, and FT-IR spectroscopy, confirming bidentate S,S′-chelation of the dithiolate ligand alongside N-coordination of 4,4′-bipyridine. Thin-film morphological studies reveal distinct nanoscale surface features, indicating ligand-dependent aggregation behavior. Electrical measurements demonstrate reproducible write-once-read-many (abbreviated as WORM) type resistive switching with low set voltages, wide memory windows, and excellent retention, highlighting their promise for non-volatile molecular memory devices. Furthermore, *in vitro* cytotoxicity assays against A-549 lung cancer cells reveal significant antiproliferative activity for selected complexes, while maintaining appreciable biocompatibility toward normal lung epithelial cells. The combined optical, electrical, and biological performances underscore the potential of dithiolate-based mixed-ligand metal complexes as versatile platforms for next-generation electronic and therapeutic applications.

**Keywords**: Mixed-ligand coordination complexes, Dithiolate ligands, 4,4′-Bipyridine, Molecular memory (WORM), Cytotoxic activity

Metal dithiolate chemistry has remained a subject of sustained scientific interest due to the remarkable structural diversity and multifunctional properties exhibited by these ligands when coordinated to transition and non-transition metal ions. Over several decades, extensive investigations have demonstrated that dithiolate-based metal complexes possess significant relevance in both inorganic chemistry and applied sciences, particularly in materials science and bioinorganic chemistry[1–4]. The strong chelating ability of sulfur donors enables the formation of thermodynamically stable complexes with intriguing electronic and redox properties.

Dithiolates and their metal complexes have found wide-ranging applications in agriculture and industry, including their use as fungicides, herbicides, bactericides, and pesticides[5–7]. Beyond biological activity, these compounds are employed as ultraviolet stabilizers for polymers, electrical insulators, semiconducting materials, and vulcanization accelerators, highlighting their technological importance[8–10]. Certain sulfur-containing compounds have also been investigated for radioprotective behavior, owing to their capacity to scavenge free radicals generated during radiation exposure[11]. Additionally, gallium and nickel dithiolate complexes have attracted attention for their anticancer potential, with *in vitro* and *in vivo* studies reporting notable cytotoxic effects at relatively low concentrations[12,13]. These versatile applications have resulted in a significant number of patents and industrial formulations based on dithiolate derivatives[14–16].

Among substituted dithiolate ligands, 1-cyano-carboethoxyethylene-2,2-dithiolate ($CED^{2-}$) has emerged as a particularly attractive system due to its conjugated framework and mixed donor

characteristics. Early foundational work established the synthesis and coordination behavior of transition-metal dithiolate complexes, providing critical insight into their structural motifs and bonding patterns[17,18]. Subsequent investigations expanded this chemistry to include nickel(II) and other first-row transition metals, revealing that $CED^{2-}$ ligands readily form chelated structures that exhibit rich electronic features and tunable properties[19–21]. Reviews on metal dithiolates have emphasized their significance as precursors for molecular conductors, optical materials, and coordination polymers[22].

In recent years, research has increasingly focused on mixed-ligand coordination systems incorporating dithiolates alongside nitrogen-donor ligands. Such mixed-ligand approaches offer enhanced control over geometry, electronic distribution, and reactivity of metal centers. Nickel(II) complexes incorporating $CED^{2-}$ together with rigid nitrogen-donor ligands such as 4,4′-bipyridine have been reported to exhibit diverse coordination modes, extended structural architectures, and enhanced thermal and chemical stability, owing to the bridging nature and strong σ-donor ability of the ligand[23–25]. Structural and spectroscopic studies have confirmed that these ligands synergistically influence metal–ligand bonding and electronic transitions, making them promising candidates for functional materials.

Parallel developments in coordination chemistry have demonstrated that mixed-ligand nickel(II) complexes exhibit noteworthy catalytic, thermal, and adsorption properties. Complexes incorporating nitrogen heterocycles have been explored for applications ranging from catalysis and dye adsorption to nanostructured material synthesis[26–29]. Detailed studies on nickel(II) systems incorporating 4,4′-bipyridine as a nitrogen-donor ligand have highlighted their distinctive reactivity patterns, coordination flexibility, and well-defined structure–property relationships arising from the ligand's rigid, bridging nature and π-conjugated framework[30–32].

In view of the extensive literature and the growing interest in multifunctional coordination compounds, the current effort focuses on the synthesis of multifunctional ligand M(II) complexes containing $CED^{2-}$ in combination with 4,4-bipyridine [$M(4,4\text{-bipyridine})_2(CED)$] (where, M = Nickel(II), Cobalt(II), Zinc(II) and Cadmium(II)). These complexes are expected to exhibit interesting optical, electrical, and biological properties. Accordingly, this study reports the preparation, spectroscopic characterization, optical behavior, current–voltage characteristics, and evaluation of cytotoxic activities of four M(II) mixed-ligand complexes. The results aim to contribute further to the understanding of structure–property relationships in dithiolate-based coordination compounds and their potential technological and biological applications.

## Experimental Section

### Materials and methods

The chemical *viz.* 4,4-bipyridine, $Ni(NO_3)_2.6H_2O$, $Zn(NO_3)_2.6H_2O$ $Co(NO_3)_2.6H_2O$, and $Cd(NO_3)_2.4H_2O$ were procured from Sigma–Aldrich and utilized without additional refinement. The synthesis of $K_2CED.H_2O$ followed a reported literature procedure[33]. Electrical conductance data for the synthesized complexes were also recorded by using digital conductivity meter (model 601). For elemental analysis (CHN) Perkin-Elmer 2400 Series II instrument was employed.

### Spectral Characterization

UV–Vis spectra were analyzed on a UV-Vis spectroscope (Shimadzu UV-1800) using a quartz cuvette (path length = 1.0 cm). Spectra were acquired in the range 250–600 nm at RT. Compounds were prepared by adding aliquots (40, 80, 140, 220 μL) of the stock solution (1mM) to solvent (DMSO), and spectra were baseline corrected against the neat solvent. The fluorescence spectra of the synthesized complexes were recorded using a PerkinElmer LS-55 fluorescence spectrometer. The infrared spectra of the ligand and the corresponding complexes **1-4** were obtained in the 400–4000 $cm^{-1}$ range using a Bruker Alpha II FT-IR spectrophotometer.

### Morphological Characterization

The thin films were prepared by a drop-casting technique. Precursor solutions of the respective formulations (**L-CED**, C1, C2, C3, and C4) were prepared in [DMSO] at a concentration of 1 mM. A fixed volume of each solution (typically 300 μL) was carefully deposited onto pre-cleaned glass substrates and allowed to dry under ambient conditions. The surface morphology of the equipped drop-casted films was recorded by a commercially obtainable field emission scanning electron microscope (FESEM) (Sigma 300, Zeiss Pvt Ltd.), working at an accelerating potential of 5 KV.

### Electrical Characterization

Electrical characterization of the compounds (**L-CED**, C1, C2, C3, and C4) has been studied in ambient situation using a Keithley source-meter

(2614B) and probe station (Everbeing C2). The DC staircase sweeps of optimized magnitude and direction were engaged in order to get the optimum current−voltage response of the devices. The I−V data were recorded with the step voltage 0.02 V per step. During measurement, compliance current (CC) was maintained at 1 mA to avoid dielectric breakdown of the compounds.

## Synthesis of complexes

### Preparation of [Ni(4,4-Bipy)$_2$(CED)] (1)

A 10 mL 4,4-Bipyridine solution of methanol (0.156g, 1 mmol) was mixed drop wise to a 20 mL aq. solution of $Ni(NO_3)_2.6H_2O$(0.1454g, 0.5 mmol). After addition, bluish green coloured solution was observed. After 10 minutes stirring, 10 mL aqueous solution of $K_2CED.H_2O$ (0.142g, 0.5.mmol) was added drop by drop to this final solution with steady stirring, an orange brown coloured precipitate was formed. After 1 hour constant shaking, the ppt was filtered off, washed with distilled water and dried in a vacuum over fused $CaCl_2$.

Yield: 0.227g (81%); Analytical Calcd ($C_{26}H_{21}N_5O_2S_2Ni$): C, 55.93; H, 3.79; N, 12.54%. Obsd: C, 55.68; H, 3.24; N, 12.12%. UV-Vis (DMSO) λmax (in nm): $K_2CED.H_2O$ (Ligand): 256, 274 nm. Complex **1**: 345, 445, 479 nm. IR ($cm^{-1}$): $K_2CED.H_2O$ (Ligand): 2190s υ(C≡N str.), 1642s υ(C=O), 1320vs, 1375vs υ(C=C), 1020s $\upsilon_{as}$(=$CS_2$), 930m $\upsilon_s$ (=$CS_2$), 886m υ(C–S str.). Complex **1**: 2986w υ(Aromatic/Aliphatic C-H str.), 2195s υ(C≡N str.), 1649s, 1597 υ(=CO), 1534s, 1371vs υ(C=C), 1025vs $\upsilon_{asm}$(=$CS_2$), 918m $\upsilon_{sym}$(=$CS_2$), 805m υ(C–S str.), 616s υ(In-plane ring deformation).

### Preparation of [Co(4,4-Bipy)$_2$(CED)] (2)

A 10 mL 4,4-Bipyridine solution of methanol (0.156g, 1 mmol) was mixed drop wise to a 20 mL aq. solution of $Co(NO_3)_2.6H_2O$(0.145g,0.5mmol). After addition orange red coloured solution was observed. After 10 minutes stirring 10 mL aqueous solution of $K_2CED.H_2O$ (0.142g 0.5 mmol) was added drop by drop to this final solution with steady stirring, an olive green coloured precipitate was formed. After 1 hour constant shaking, the ppt was filtered off, washed with distilled water and dried in a vacuum over fused $CaCl_2$.

Yield: 0.202g (72%); Analytical Calcd. ($C_{26}H_{21}N_5O_2S_2Co$): C, 55.91; H, 3.79; N, 12.54%. Observed: C, 55.67; H, 3.64; N, 12.17%. UV-Vis (DMSO) λmax (in nm): 337, 445 nm. IR ($cm^{-1}$): 2975w υ(Aromatic/Aliphatic C-H str.), 2186s υ(C≡N str.), 1646s, 1599vs υ(C=O), 1532s, 1407vs υ(C=C), 1029s $\upsilon_{asm}$(=$CS_2$), 929m $\upsilon_{sym}$(=$CS_2$), 807m υ(C–S str.), 627w υ (In-plane ring deformation).

### Preparation of [Zn(4,4-Bipy)$_2$(CED)] (3)

A 10 mL 4,4-Bipyridine solution of methanol (0.156g, 1 mmol) was mixed drop wise to a 20 mL aq. solution of $Zn(NO_3)_2.6H_2O$(0.1487g 0.5 mmol). After addition light straw coloured solution was observed. After 10 minutes stirring, 10 mL aqueous solution of $K_2CED.H_2O$ (0.142g 0.5 mmol) was added drop by drop to this final solution with steady stirring, a light yellow coloured precipitate was formed. After 1 hour constant shaking, the ppt was filtered off, washed with distilled water and dried in a vacuum over fused $CaCl_2$.

Yield: 0.198g(70%); Analytical Calcd ($C_{26}H_{21}N_5O_2S_2Zn$): C, 55.27; H, 3.75; N, 12.40%. Obsd: C, 55.45; H, 3.73; N, 12.42%. UV-Vis (DMSO) λmax (in nm): 312, 339 nm. IR ($cm^{-1}$): 2947w υ(Aromatic/Aliphatic C-H str.), 2197vs υ(C≡N str.), 1675w, 1597vs υ(C=O), 1536s, 1372vs υ(C=C), 1020s $\upsilon_{asm}$(=$CS_2$), 928m $\upsilon_{sym}$(=$CS_2$), 806m υ(C–S str.), 637vs, 621s υ(In-plane ring deformation).

### Preparation of [Cd(4,4-Bipy)$_2$(CED)] (4)

A 10 mL 4,4-Bipyridine solution of methanol (0.156g, 1 mmol) was mixed drop wise to a 20 mL aq. solution of $Cd(NO_3)_2.4H_2O$(0.154g 0.5 mmol). After addition light straw coloured solution was observed. After 10 minutes stirring, 10 mL aqueous solution of $K_2CED.H_2O$ (0.14171g 0.5mmol) was added drop by drop to this final solution with steady stirring, a light yellow coloured precipitate was formed. After 1 hour constant shaking, the ppt was filtered off, washed with distilled water and dried in a vacuum over fused $CaCl_2$.

Yield: 0.204g (66%); Analytical Calcd ($C_{26}H_{21}N_5O_2S_2Cd$): C, 51.02; H, 3.46; N, 11.44%. Obsd: C, 55.68; H, 3.48; N, 11.46%. UV-Vis (DMSO) λmax (in nm): 342 nm. IR ($cm^{-1}$): 2978w υ(Aromatic/Aliphatic C-H str.), 2201s υ(C≡N str.), 1603s υ(C=O), 1533s υ(C=C), 1022s $\upsilon_{asm}$(=$CS_2$), 924m $\upsilon_{sym}$(=$CS_2$), 808s υ(C–S str.), 628s υ(In-plane ring deformation).

## Cytotoxicity assay

The cytotoxic potential of the synthesized samples was evaluated using the standard MTT colorimetric

assay, which measures cellular metabolic activity rooted in the reduction of MTT to insoluble blue formazan crystals by mitochondrial succinate dehydrogenase in viable cells. Human lung adenocarcinoma (A-549) and normal human lung epithelial (BEAS-2B) cell lines were cultured in Dulbecco's Modified Eagle Medium (DMEM) supplemented with 10% (v/v) fetal bovine serum (FBS) and maintained at 37°C in a humidified incubator with 5% $CO_2$. Cells at approximately 80% confluence were harvested and seeded into 96-well culture plates at a density of $1 \times 10^4$ cells per well, followed by overnight incubation to allow cell attachment. After initial 4-hrs incubation, the culture medium was replaced with serum-free DMEM. The cells were then treated with **L-CED** and complexes **1**–**4** at different concentrations (10 ng $mL^{-1}$, 500 ng $mL^{-1}$, 1 µg $mL^{-1}$, and 50 µg $mL^{-1}$). *Cis*-platin (0.5 mg $mL^{-1}$) was used as a reference drug for A-549 cells. Following 24 hours of treatment, the medium was then replaced with fresh serum-free DMEM, and MTT solution (12 mM, 10 µL) was added to each well. Upon completion of the 4 hrs incubation period, the supernatant was removed, and the insoluble formazan crystals were dissolved in 50 µL of DMSO. Absorbance readings were obtained at 540 nm using a Synergy H1 microplate reader[34,35].

## Results and Discussion

### Synthesis of complexes

When Metal nitrates were treated with nitrogen donor (4,4-Bipyridine) and sulphur donor like 1,1-dithiolate namely 1-cyano-1-carboethoxyethylene-2,2-dithiolate *i.e.* ($CED^{2-}$) Under various experimental conditions, the product formed was found to have the same composition, [M(4,4-bipyridine)$_2$ (CED)] (where, M = Ni(II), Co(II), Zn(II) and Cd(II)). The analytical data suggest that the successful synthesis of four mixed ligand complexes having different metal ions with S and N-donors (Scheme 1). All the synthesized mixed ligand complexes are decomposed below 240ºC and are soluble in DMF solvent along with DMSO solvent but are not soluble in some common organic solvent like Acetone, $CCl_4$, $CHCl_3$, $CH_3OH$, $C_2H_5OH$.

### Molar conductance study

The electrical conductance values of the four synthesized mixed-ligand complexes measured in DMF solution were in the range of 14.2–22.5 µS, indicating their non-electrolytic nature[36].

## Spectroscopic Characterization

### UV-Vis absorption spectra

The electronic absorption spectra (UV–Vis) of the five compounds (**L-CED**, C-1, C-2, C-3 and C4) were recorded to evaluate the electronic transitions arising from the ligands and the metal-ligand interactions. Fig. 1 represents the electronic absorption spectra (UV–Vis) of the Compounds which were obtained by incremental additions of Compound (40, 80, 140 and 220 µL). Peak positions that were identified visually from the spectra (Fig. 1) are summarized in Table 1 and described below.

**L-CED** exhibited a strong absorption band centred at ≈256 nm, accompanied by a weaker shoulder at ≈274 nm. These peaks are typical of ligand-centred transitions and may be assigned to allowed π → π* transitions of the ligand backbone. Compound C-1 exhibited three distinguished bands located at ≈345

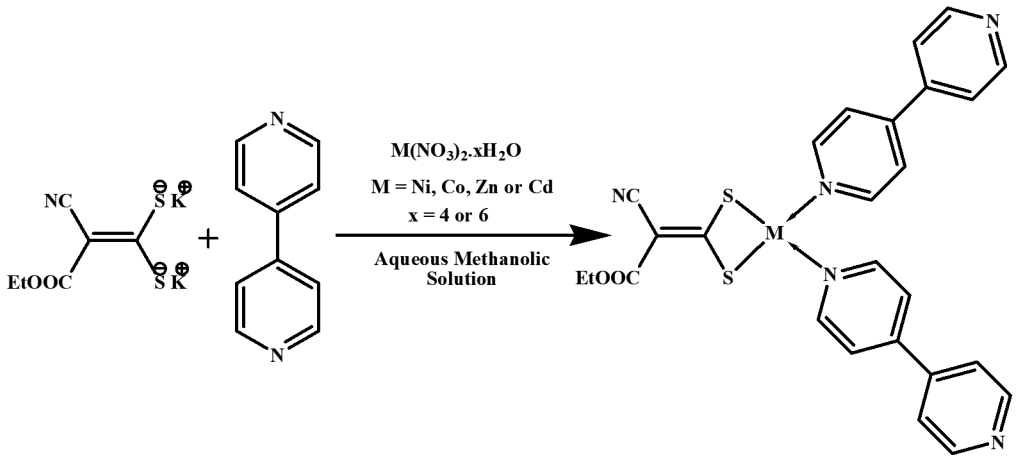


Scheme 1 — Schematic representation of the synthesis of complexes **1**, **2**, **3**, and **4**

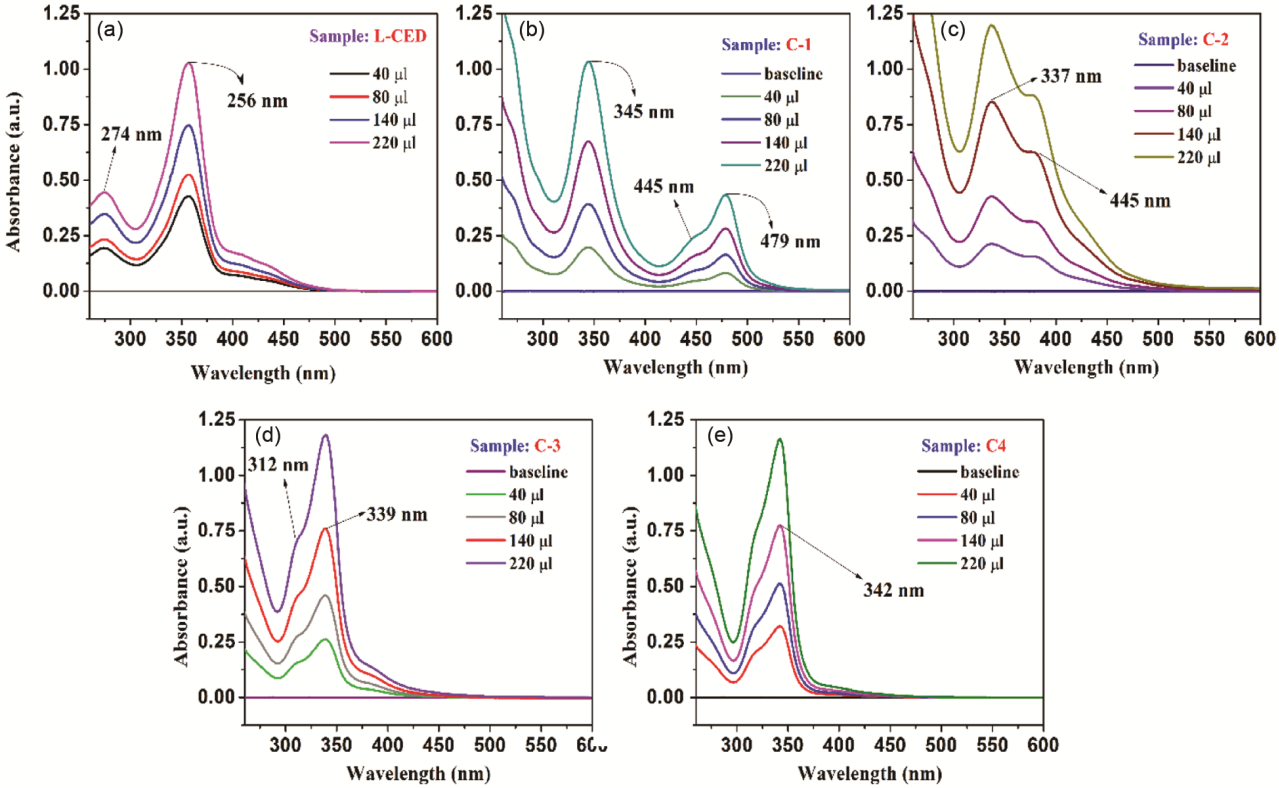


Fig. 1 — The electronic absorption spectra (UV–Vis) of (a) **L-CED**, (b) C-1, (c) C-2, (d) C-3 and (e) C4 recorded between 250 and 600 nm. Spectra obtained after incremental additions of Compound (40, 80, 140 and 220 µL) are shown. Peak positions (λmax) are indicated on the plots

Table 1 — UV-Vis Spectra peak positions

| Compd | Observed λmax (nm) | Assignment |
|---|---|---|
| **L-CED** (a) | 256, 274 | Ligand π → π* |
| C-1 (b) | 345, 445, 479 | Ligand-perturbed π → π*; low-energy CT or d–d |
| C-2 (c) | 337, 445 | Ligand π → π* (coordination shifted); low-energy CT/d–d |
| C-3 (d) | 312, 339 | Ligand π → π* (vibronic splitting / multiple ligand environments) |
| C4 (e) | 342 | Ligand π → π* (coordination influenced) |

nm, 445 nm and 479 nm. The low-energy bands (445 and 479 nm) displayed broader profiles relative to the higher-energy band. The band at ≈345 nm can be a ligand-centred π → π* transition that was bathochromically shifted by coordination. The absorptions at 445 nm and 479 nm may be assigned to metal-related transitions. C-2 displayed a pronounced band at ≈337 nm and a broad low-energy peak centred at ≈445 nm. The 337 nm band may be attributed to a ligand-centred π → π* transition that is red-shifted relative to the free ligand reference (**L-CED**). For C-3 two main bands are observed at ≈312 nm and ≈339 nm which resembles ligand-centred π → π* transitions, where the dual peaks indicates two ligand electronic environments or vibronic splitting of the same transition. C4 exhibited a single dominant absorption centred at ≈342 nm which is suggestive of a ligand-related π → π* transition that was influenced by coordination to the metal center.

## Fluorescence study

The fluorescence spectra of the ligand (**L-CED**) and its corresponding coordination complexes (**C-1** to **C-4**) were recorded in the solution state at laboratory temperature, as depicted in Fig. 2a-e. The ligand **L-CED** displayed a prominent emission maximum at 416 nm when excited at 356 nm, which originated from the π-π* transition of the conjugated coumarin-ethoxy framework. Upon metal coordination, distinct spectral modifications were observed, indicating perturbation of the electronic structure. Complex C-1 displayed two emission bands at 383 nm and 416 nm

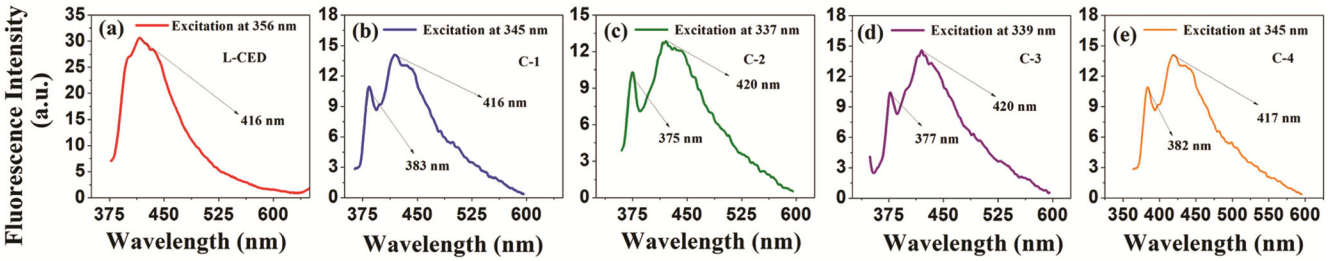


Fig. 2 — Fluorescence emission spectra of (a) **L-CED**, (b) C-1, (c) C-2, (d) C-3, and (e) C-4 recorded in the solid state at RT, showing excitation-dependent emissions with distinct peak positions, confirming modulation of the electronic structure upon metal coordination.

under 345 nm excitation, while complex C-2 exhibited emissions at 375 nm and 420 nm upon excitation at 337 nm. Complex C-3 showed similar dual emission features at 377 nm and 420 nm with an excitation wavelength of 339 nm, and complex C-4 presented emission maxima at 382 nm and 417 nm under 345 nm excitation. The observed blue-shifted or red-shifted transitions relative to the free ligand could be attributed to variations in the metal–ligand charge-transfer (MLCT) as well as intraligand charge-transfer (ILCT) interactions upon complex formation. Moreover, the presence of dual emission bands in all complexes suggests the coexistence of locally excited and charge-transfer states. The minor spectral shifts and intensity variations further imply that coordination alters the electron density distribution within the coumarin core, affecting its radiative decay pathways. These results confirm that metal complexation modulates the photophysical behavior of the ligand while retaining its luminescent characteristics, thereby supporting its potential utility in optoelectronic and memory device applications.

## IR spectroscopy

The infrared spectral data of the synthesized multifunctional-ligand complexes [M(4,4′-bipy)$_2$(CED)] (where M = Ni(II), Co(II), Zn(II), and Cd(II)) clearly confirm the coordination behavior of the cyanocarboethyldithiocarbamate ($CED^{2-}$) and 4,4′-bipyridine ligands towards the respective metal(II) ions. The free ligand $K_2CED{\cdot}H_2O$ shows prominent absorption bands at 2190 cm$^{-1}$ (νC≡N), 1642 cm$^{-1}$ (νC=O), 1320 and 1375 cm$^{-1}$ (νC=C), 1020 and 930 cm$^{-1}$ (asymmetric and symmetric ν=CS$_2$), and 886 cm$^{-1}$ (νC–S). Upon coordination, distinct spectral changes are observed in all the complexes, confirming successful metal–ligand interaction. In the complexes, the ν(C≡N) stretching frequency appears between 2186 and 2201 cm$^{-1}$, shifted slightly to higher values compared with the free ligand, which indicates a decrease in π-back bonding from the metal center to the cyano group and partial delocalization of the C≡N electron density over the ligand framework. Such a shift suggests that the cyano nitrogen may not be directly coordinated, but its electronic environment is perturbed due to metal–ligand interactions through adjacent donor atoms[37].

The carbonyl stretching vibration, which appears at 1642 cm$^{-1}$ in the free ligand, is found in the range of 1597–1675 cm$^{-1}$ in the complexes, suggesting a change in the electronic distribution around the carbonyl group and a possible weak coordination. The most diagnostic feature confirming coordination arises from the $\nu_{asm}$(=CS$_2$) and $\nu_{sym}$(=CS$_2$) bands, which appear in the free ligand at 1020 and 930 cm$^{-1}$, respectively, but are shifted to slightly higher wave numbers (1020–1030 cm$^{-1}$ and 918–929 cm$^{-1}$) in the metal complexes. The observed separation ($\Delta\nu = \nu_{asm} - \nu_{sym} \approx 90$–$110$ cm$^{-1}$) is characteristic of bidentate chelating coordination through both sulfur atoms of the dithiocarbamate moiety, as established in earlier reports on similar systems[38,39].

The ν(C–S) band, which appears at 886 cm$^{-1}$ in the free ligand, shifts to a lower frequency region (805–808 cm$^{-1}$) upon complexation, confirming the direct involvement of sulfur atoms in metal coordination. Additionally, the bands corresponding to aromatic/aliphatic ν(C–H) stretching vibrations appeared as weak bands around 2947–2986 cm$^{-1}$, typical of coordinated 4,4′-bipyridine. The in-plane ring deformation modes appearing at 616–637 cm$^{-1}$ in the complexes correspond to the characteristic vibrations of 4,4′-bipyridine, confirming that the ligand coordinates through its nitrogen donor atoms without significant perturbation of the aromatic ring. Across the series, slight variations in the positions of ν(C≡N) and ν(C=O) vibrations (Ni<Co< Zn<Cd) reflect the differences in ionic radii and electronegativity of the metal centers. The higher ν(C≡N) and lower ν(C=O) in the Cd(II) complex

suggest weaker π-backbonding and a relatively more ionic metal–ligand interaction compared to the Ni(II) and Co(II) analogues, which exhibit slightly stronger bonding characteristics. This trend aligns with literature reports on similar dithiocarbamate–bipyridine complexes of first-row and second-row transition metals[40,41].

Thus, the IR spectral evidence collectively confirms that in all complexes, the CED ligand coordinates in a bidentate S,S′-chelation mode, while the 4,4′-bipyridine acts as a neutral N-donor ligand, leading to square planar coordination geometries around the metal centers. These spectral features are consistent with reported mixed-ligand coordination compounds containing dithiocarbamate and bipyridyl moieties, supporting the formation of stable metal–ligand frameworks[37,38,40,42].

## Morphological Characterization

The surface morphology of the drop-casted thin films was systematically examined using field-emission scanning electron microscopy (FESEM). Representative micrographs of the five Compounds (**L-CED**, **C1**, **C2**, **C3**, and **C4**) recorded at a magnification of 20,000X are shown in Fig. 3. Distinctive morphological features were observed across the Compounds, reflecting the influence of material composition and deposition conditions on the

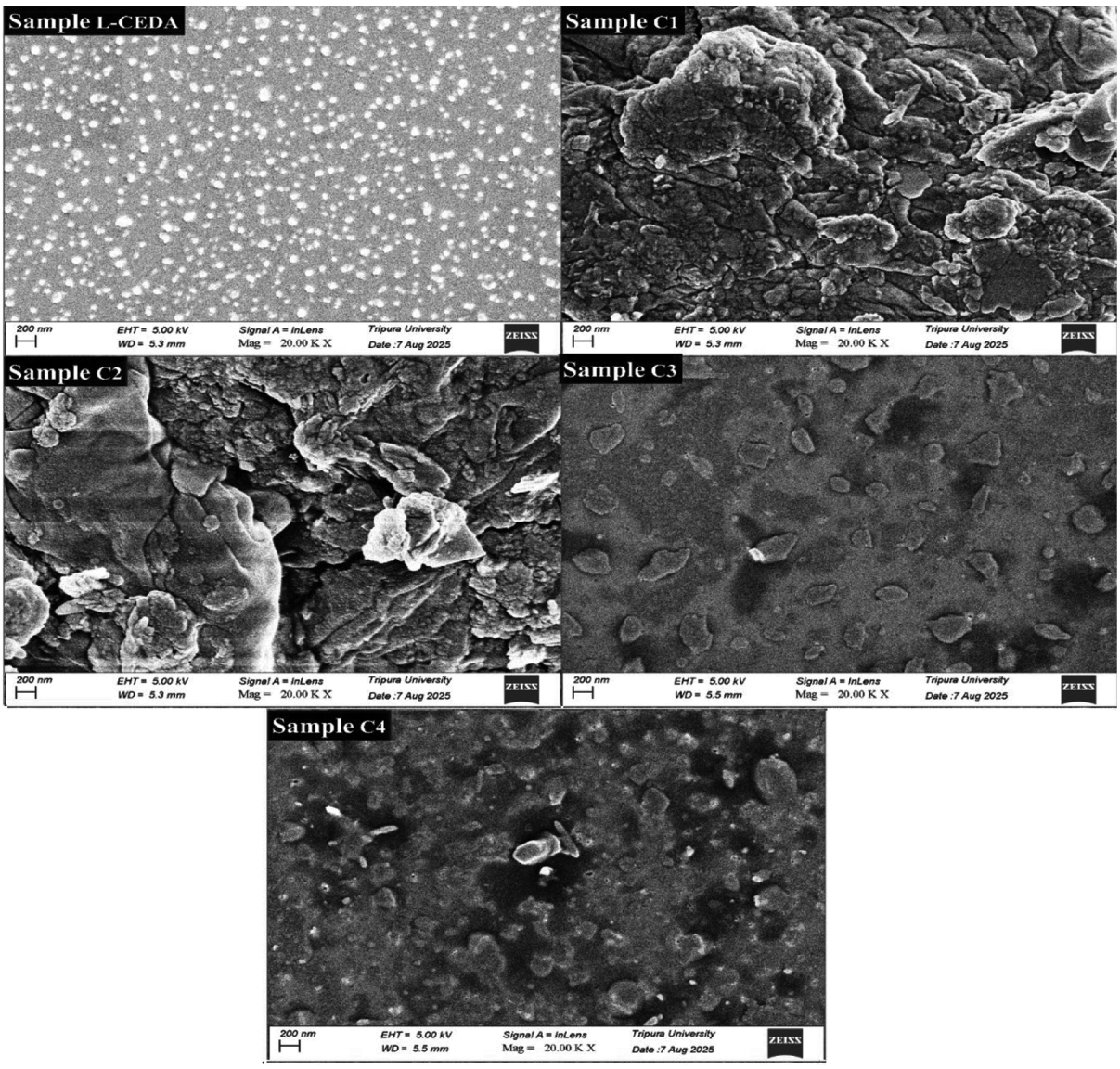


Fig. 3 — FESEM micrograms of the Surface morphology of the Compounds **L-CED**, C-1, C-2, C-3 and C-4 in drop-casted thin-films obtained by at 20,000X magnification operating at accelerating potential of 5KV.

nanoscale surface topography. The SEM image of Compound **L-CED** reveals a uniform distribution of well-defined nanoscale domains scattered across the film surface. The spherical to quasi-spherical features appear consistently separated, suggesting the formation of discrete nucleation centers during film growth. The high surface coverage with homogeneous particle distribution points to controlled nucleation and limited agglomeration. Compound C1 displays a markedly different morphology compared to **L-CED**. The surface is dominated by large, irregularly shaped aggregates and roughened topographies. These micron-sized clusters appear to arise from uncontrolled agglomeration.

In Compound C2, the surface consists of broad, sheet-like structures layered across the film. The flake-like morphology indicates extensive aggregation and partial fusion of primary particles, forming larger domains with limited nanoscale definition. Compared to C1, the agglomerates here are more compact, with platelet-like fragments embedded in the film matrix. These morphological features hint at strong interparticle interactions that promote secondary structure formation. Compound C3 demonstrates a relatively smoother surface morphology, with scattered nanoscale patches distributed throughout the film. The features appear less aggregated than in C1 and C2, but the surface still lacks the uniformity observed in **L-CED**. The granular morphology, with isolated islands embedded in the matrix, suggests partial suppression of agglomeration. The SEM image of Compound C4 shows a fine-grained, densely packed nanostructure, with small particles distributed across the surface in relatively uniform fashion. While some agglomerates are still visible, they are smaller and more dispersed compared to C1 and C2. The film demonstrates improved homogeneity, bridging the gap between the highly uniform **L-CED** and the more heterogeneous C1–C3 Compounds. The presence of nanoscale domains suggests enhanced stabilization during drop casting, leading to better-controlled nucleation and growth.

## Electrical Characterization and Memory Behavior

The current–voltage (I–V) behaviours of the made-up molecular devices based on **L-CED**, **C-1**, **C-2**, **C-3** and **C-4**, with device structure Au/S/ITO (S representing the corresponding Compound), were examined under a consecutive sweeping sequence (0 → +2 V → 0 → −2 V → 0 → +2 V). The IV responses of the Compounds are presented in Fig. 4. As observed from the figure (Fig. 4), all the

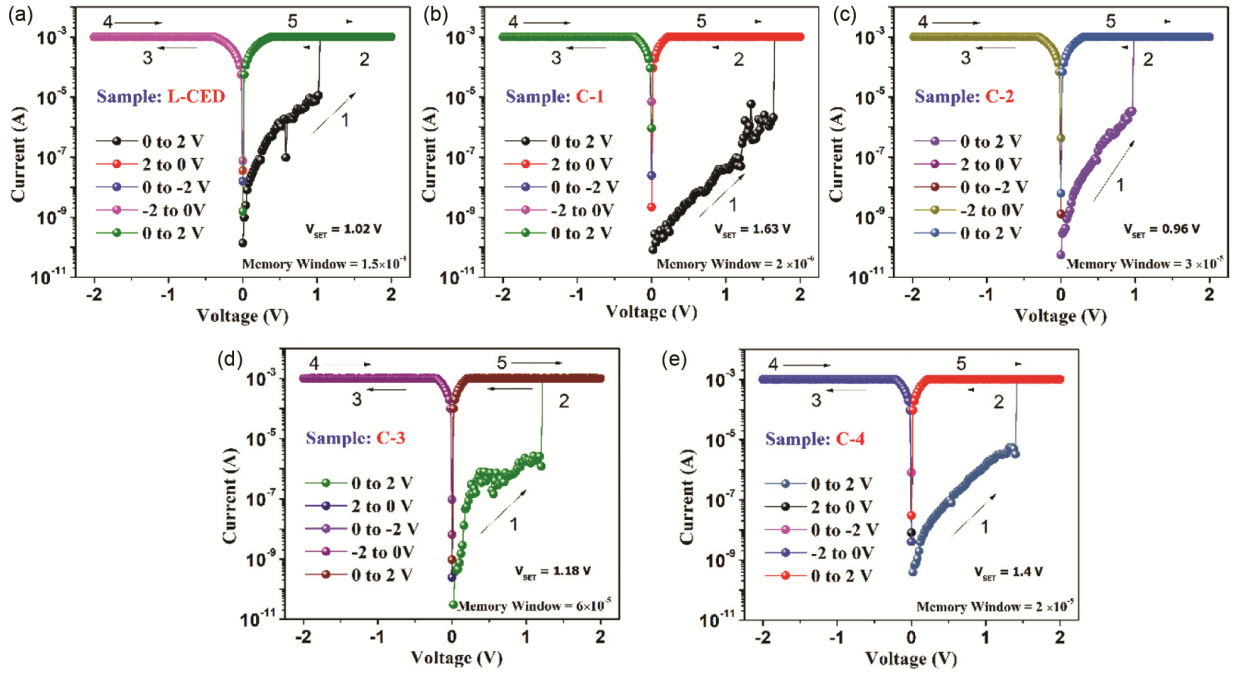


Fig. 4 — Current–voltage (I–V) behaviours of the molecular devices fabricated with (a) **L-CED**, (b) C-1, (c) C-2, (d) C-3 and (e) C-4. All measurements were performed under a consecutive bipolar voltage sweep (0 → +2 V → 0 → −2 V → 0 → +2 V). Distinct hysteresis loops confirm reproducible WORM type resistive switching behaviour in each case. The extracted set voltages ($V_{SET}$) and corresponding memory windows are indicated in the plots.

Table 2 — Summary of resistive switching parameters

| Compd | Set Voltage (V) | Memory Window | Read Endurance | Retention time (s) |
|---|---|---|---|---|
| **L-CED** | 1.02 | $1.5\times10^4$ | $10^3$ | $10^3$ |
| C-1 | 1.63 | $2\times10^6$ | $10^3$ | $10^3$ |
| C-2 | 0.96 | $3\times10^5$ | $10^3$ | $10^3$ |
| C-3 | 1.18 | $6\times10^5$ | $10^3$ | $10^3$ |
| C-4 | 1.40 | $2\times10^5$ | $10^3$ | $10^3$ |

compounds exhibit distinct Write-Once-Read-Many (WORM) type resistive switching behavior with notable variation in set voltage ($V_{SET}$), current levels, and memory windows[43]. The switching parameters are summarized in Table 2.

The device incorporating **L-CED** exhibited WORM characteristics with a $V_{SET}$ of ≈1.02 V. A sharp increase in current was observed when the applied bias reached $V_{SET}$, reflecting an irreversible change from the high-resistance (HRS) to the low-resistance state (LRS)[44]. The current levels remained stable during subsequent sweeps. The memory window was found to be $\approx1.5\times10^4$ which indicates robust separation between the ON and OFF states Compounds C-1, C-2, C-3 and C-4 also exhibited similar WORM type resistive switching with $V_{SET}$ values of 1.63 V, 0.96 V, 1.18 V and 1.40 V, respectively. The corresponding memory windows were found to be $2\times10^6$, $3\times10^5$, $6\times10^5$ and $2\times10^5$, respectively. The $V_{SET}$ values varied between 0.96 and 1.63 V across the complexes. C-2 required the lowest set voltage, implying easier carrier injection, while C-1 required the highest voltage, suggesting stronger barriers for conduction[45].

The read endurance behaviour of the fabricated molecular devices was evaluated by monitoring the resistance states at a read voltage of 0.1 V for $10^3$ consecutive cycles. Fig. 5a–e shows the variation of the high-resistance state ($R_{HRS}$) and low-resistance state ($R_{LRS}$) for Compounds **L-CED**, **C-1**, **C-2**, **C-3** and **C-4**, respectively. The endurance test revealed stable switching for most cycles, with $R_{LRS}$ at ~$10^3$–10^4 Ω and $R_{HRS}$ at ~$10^8$ Ω. A slight fluctuation in $R_{LRS}$ was observed at higher cycle counts, but the ON/OFF ratio remained distinguishable.

The non-volatile stability of the resistive switching devices was further confirmed by data retention measurements conducted at a read voltage of 0.1 V for $10^3$ s, as shown in Fig. 6a-e. All devices maintained well-separated resistance states over the entire retention period, with $R_{LRS}$ remaining in the range of $10^3$–$10^4$ Ω and $R_{HRS}$ stabilized between $10^8$-$10^{10}$ Ω. The absence of noticeable degradation or convergence of the two states during the test demonstrates excellent long-term stability and reliable memory retention for both the ligand (**L-CED**) and coordination complex devices (**C-1** to **C-4**). These results validate the robust non-volatile memory behaviour of the fabricated molecular systems[46,47].

## Cytotoxic activities

The graph in Fig. 7 indicates that **L-CED** has a noteworthy effect on the A-549 lung cancer cell line at all the mentioned concentrations. The cytotoxicity is significant at 500 ng/mL for compound 2 and compound 3 with a significance level of 0.001. On the other hand, when the cells were exposed to a 1 µg/mL concentration, the cytotoxicity against compounds 2, 3, and **L-CED** was drastically altered. The highest cytotoxicity has been observed for the concentration of 50 µg/mL against **L-CED**, compound 2 and compound 3 at a very significant level. **L-CED**, compound 2 and compound 3 were found to have viable cell percentages of 36.34%, 32.27% and 20.61%, respectively.

In a recent study, the coordination chemistry of 1-cyano-carboethoxyethylene-2,2-dithiolate ($CED^{2-}$) compounds has gained significant attention regarding its anticancer potential against the A-549 (lung adenocarcinoma) cell line[35]. Furthermore, in a study, it has been shown that bipyridine amide (BPA-B9) shows anticancer activity by inhibiting pRXRα-PLK1 interaction and inducing RXRα-dependent mitotic arrest. Its pharmacokinetics are superior to lead XS-060, and it has significant *in vivo* efficacy without significant side effects, making it a promising drug candidate for further development[48]. The aforesaid results suggest that the **L-CED**, compound 2 and Compound 3 may be our compound of interest for designing and developing new therapeutics against different cancer cell lines because they comprise a bipyridine molecule. Although the precise mechanism of action by which compounds 2 and 3 impart cytotoxicity is not included in the current study, it may be stated that Compound 3 has the most cytotoxic effect on the A549 lung cancer cell line.

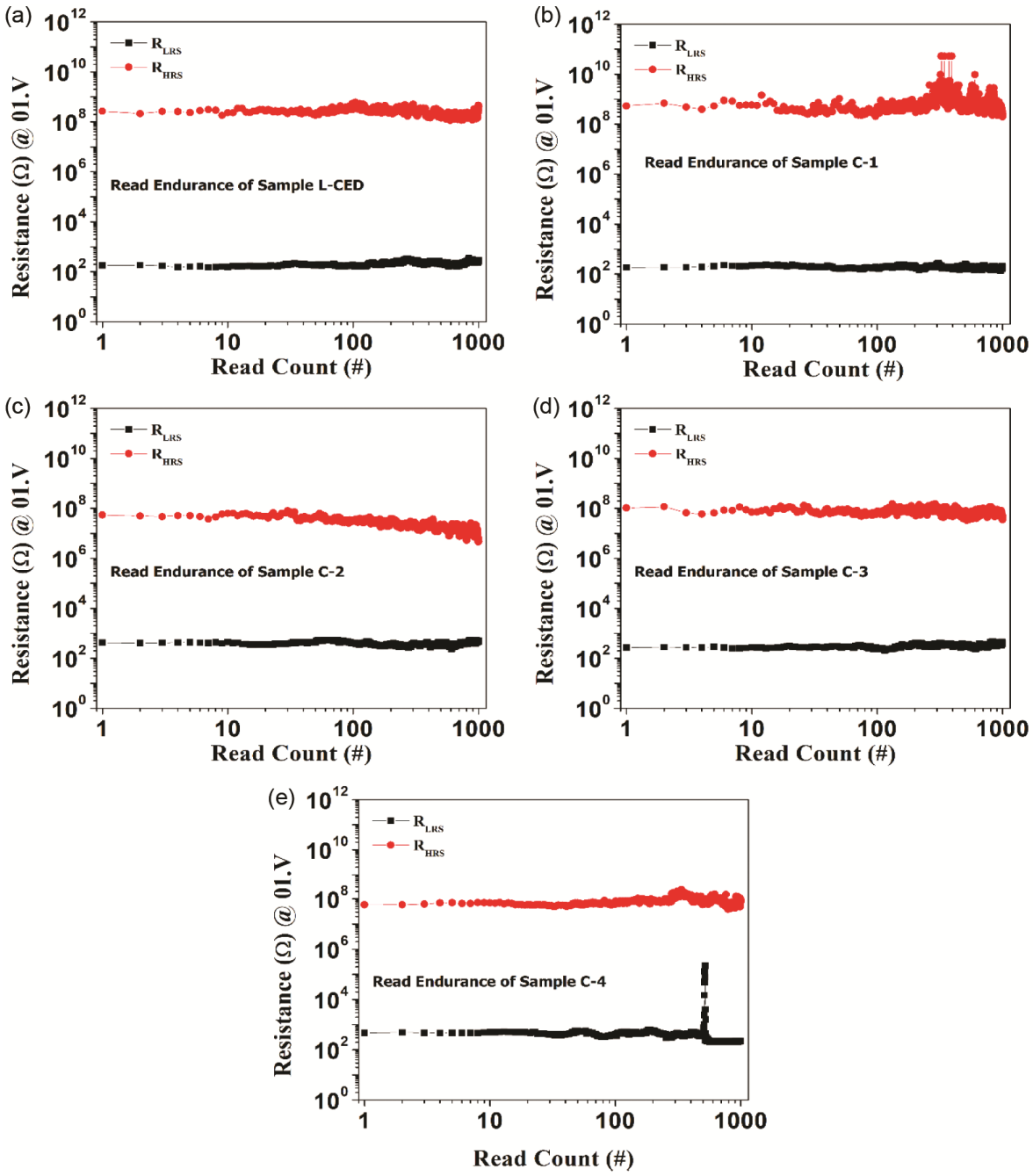


Fig. 5 — Read endurance characteristics of the fabricated devices measured at a read voltage of 0.1 V for $10^3$ consecutive cycles: (a) **L-CED**, (b) C-1, (c) C-2, (d) C-3, and (e) C-4. Both low-resistance state ($R_{LRS}$) and high-resistance state ($R_{HRS}$) are plotted, demonstrating stable resistive switching behaviour across repeated cycles with clear separation between the two states.

To find out if these substances have any effect on normal human lung epithelial cells (Beas2B), another MTT assay has been carried out. The assay was performed as described earlier. From the above graph in Fig. 8 it can be interpreted that although compound showed significant effect against Beas 2B cell line at various concentration like 10 ng/mL, 500 ng/mL and 1 µg/mL, but at 50 µg/mL almost all the compound showed but with a minimum significant difference at a level of 0.01 and 0.05. All the compounds could be a good drug candidate since approximately 70 percent of Beas 2B cells are viable at highest concentration (50 µg/mL).

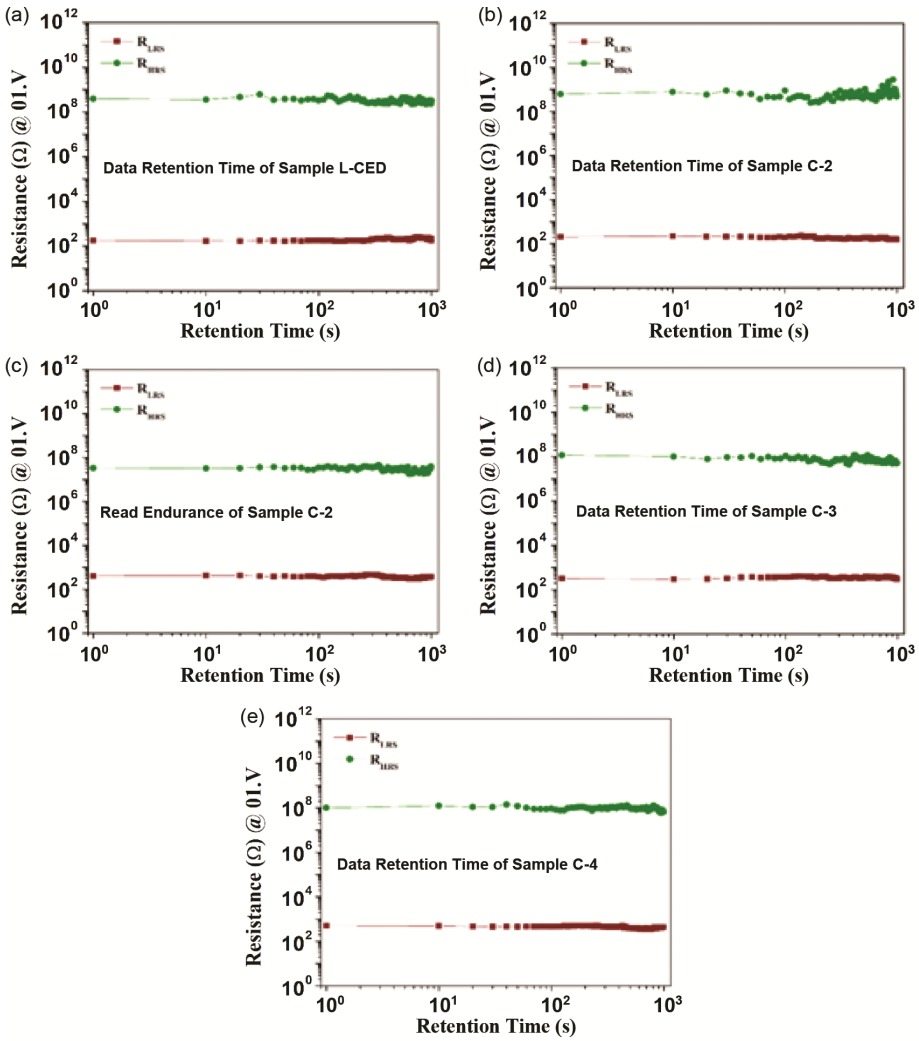


Fig. 6 — Data retention characteristics of (a) Compound **L-CED**, (b) Compound C-1, (c) Compound C-2, (d) Compound C-3, and (e) Compound C-4 measured at a read voltage of 0.1 V for $10^3$ s, showing stable separation between $R_{LRS}$ and $R_{HRS}$ without noticeable degradation, confirming reliable non-volatile memory performance.

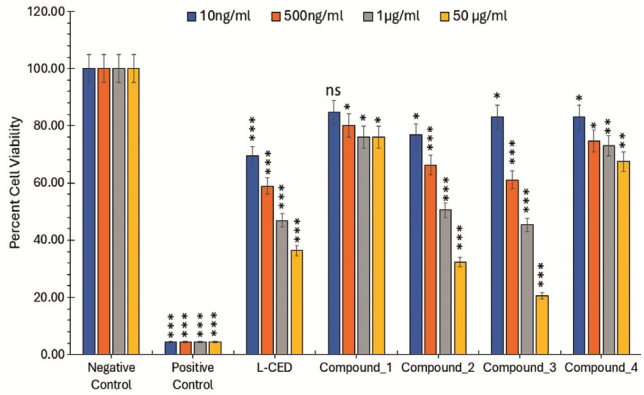


Fig. 7 — One-way ANOVA with Tukey's post hoc analysis demonstrated statistically significant differences between the control and treatment groups, represented as ***p < 0.001, *p < 0.01, p < 0.05, and ns (not significant).

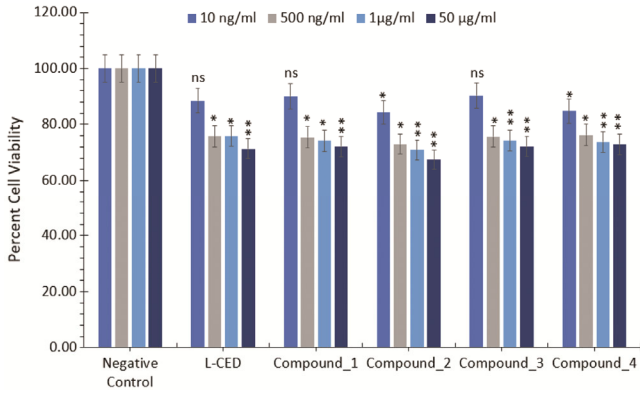


Fig. 8 — One-way ANOVA followed by Tukey's post hoc analysis revealed statistically significant differences between the control and treatment groups, represented by ***p < 0.001, *p < 0.01, p < 0.05, and ns (not significant).

## Conclusions

In summary, a series of mixed-ligand M(II) complexes (M = Ni, Co, Zn and Cd) incorporating the sulfur-rich 1-cyano-carboethoxyethylene-2,2-dithiolate ($CED^{2-}$) and the rigid nitrogen-donor ligand 4,4′-bipyridine were successfully synthesized and comprehensively characterized. Spectroscopic analyses confirmed the bidentate S,S′-chelation of the dithiolate ligand along with N-coordination of 4,4′-bipyridine, leading to stable coordination frameworks. Optical studies revealed coordination-induced modulation of electronic transitions and luminescent behavior, while morphological investigations demonstrated distinct nanoscale surface features in the fabricated thin films. Electrical measurements established reproducible write-once-read-many (WORM) type resistive switching with low operating voltages, wide memory windows, and good endurance and retention characteristics, underscoring the suitability of these complexes for non-volatile molecular memory applications. Furthermore, *in vitro* cytotoxicity studies indicated promising anticancer activity of selected complexes against A-549 lung cancer cells, with comparatively lower toxicity toward normal lung epithelial cells. Collectively, the results highlight the multifunctional nature of dithiolate-based mixed-ligand metal complexes and demonstrate their potential as versatile candidates for future applications in molecular electronics and bioinorganic therapeutics.

## Supplementary Information

Supplementary information is available in the website https://nopr.niscpr.res.in/handle/123456789/58776.

## Acknowledgements

The authors gratefully acknowledge the Science and Engineering Research Board (SERB), Department of Science and Technology (DST), Government of India, for financial support under Sanction Order No. EEQ/2021/000257 dated 25 February 2022.

## Conflicts of interest

The authors declare that there are no conflicts of interest.

## References

1 McCleverty J A, *Prog Inorg Chem,* 10 (1968) 49.
2 Eisenberg R, *Coord Chem Rev*, 19 (1976) 1.
3 Stiefel E I & Eisenberg R, *Prog Inorg Chem*, 52 (2004) 1.
4 Coucouvanis D, *Prog Inorg Chem,* 11 (1970) 233.
5 Burns R P & McAuliffe C A, *Adv Inorg Chem Radiochem*, 23 (1980) 211.
6 Nieuwenhuizen P J, Ehlers A W, Haasnoot J G, Janse S R, Reedijk J & Baerends E J, *J Am Chem Soc,* 121 (1999) 163.
7 Reedijk J, *Coord Chem Rev,* 166 (1997) 189.
8 O'Brien P, Walsh J R, Watson I M, Motevalli M & Henriksen L, *J Chem Soc Dalt Trans,* (1996) 2491. (https://doi.org/10.1039/DT9960002491).
9 Pike R D, Cui H, Kershaw R, Dwight K, Wold A, Blanton T N, Wernberg A A & Gysling H J, *Thin Solid Films*, 224 (1993) 221.
10 O'Brien P, Walsh J R, Watson I M, Hart L & Silva S R P, *J Cryst Growth*, 167 (1996) 133.
11 Mukhomorov V K, *Radiobiologiya*, 26 (1986) 560.
12 Navarro M et al, *Inorg Chem,* 43 (2004) 267
13 Kostova I, *Curr Med Chem,* 13 (2006) 1085.
14 Chem Abstr, 100 (1984) 115000a.
15 Chem Abstr, 102 (1985) 31934m.
16 Chem Abstr, 106 (1987) 67474h.
17 Coucouvanis D, Hollander F J & Caffery M L, *J Am Chem Soc*, 96 (1974) 4682.
18 Jensen K A & Henriksen L, *Acta Chem Scand*, 22 (1968) 1107.
19 Geary W J, *Coord Chem Rev*, 7 (1971) 81.
20 McCleverty J A, Orchard D G & Smith K, *J Chem Soc A*, (1971) 707.
21 Abram U, dietzsch W & Kirmse R, *Z Chem,* 22 (1982) 305.
22 Cassoux P, Valade L, *Coord Chem Rev,* 178–180 (1998) 931.
23 Batten S R & Robson R, *Angew Chem Int Ed,* 37 (1998) 1460.
24 Khlobystov A N, Blake A J, Champness N R, Lemenovskii D A, Majouga A G, Zyk N V & Schröder M, *Coord Chem Rev,* 222 (2001) 155.
25 Zhang J, Chen S M, Wu T, Zhou Y F & Feng P Y, *Inorg Chem,* 44 (2005) 2757.
26 Dağlı Ö, Kose D A, Icten O, Avci G A & Sahin O, *J Therm Anal Calorim,* 136 (2019) 1467.
27 Dzhardimalieva G I & Uflyand I E, *Inorg Mater Appl Res,* 7 (2017) 422.
28 Khan M I & Nair B K, *Inorg Chem Comm,* 31 (2013) 78.
29 Batten S R, Neville S M & Turner D R, *Coordination Polymers: Design, Analysis and Application*, Royal Society of Chemistry, Cambridge (2009).
30 Zhang J, Chen S M, Wu T & Feng P Y, *Inorg Chem,* 43 (2004) 5806.
31 Blake A J, Champness N R, Hubberstey P, Li W S, Withersby M A & Schröder M, *Coord Chem Rev,* 183 (1999) 117.
32 Das M C, Xu H & Wang X S, *Dalton Trans,* 38 (2009) 8100.
33 Jensen K A & Henriksen L, *Acta Chem Scand*, 22 (1968) 1107.
34 Basak S, Sengupta A, Modak S, Kumar A, Maiti D & Das R, *Mater Chem Phys*, 326 (2024) 129774.
35 Debnath P, Das A, Hussain S A, Deb R, Maiti D, Modak S, Acharya S, Bhattacharya A & Bhowmik K L, *Indian J Chem*, 64 (2025) 528.
36 Das A, Hussain S A, Banik H, Maiti D, Aktar T, Acharya S & Debnath P, *Asian J Chem,* 36 (2024)1348.
37 Balachandran C, Hirose M, Tanaka T, Zhu J J, Yokoi K, Hisamatsu Y, Yamada Y & Aoki S, *Inorg Chem,* 62 (2023) 14615.).

38 Nath M, Vats M & Roy P, *J Coord Chem,* 55 (2002) 883
39 Nakamoto K, *Infrared and Raman Spectra of Inorganic and Coordination Compounds*, 6th ed, (Wiley, New York), 2009.
40 Khandar A A, Shaabani B, Mague J T & Mohammadnezhad G, *Polyhedron*, 52 (2013) 324
41 Rahman M H, Hossain M S, Das A, Molla M A H, Islam M A & Hossain M A, *Inorg Chim Acta*, 543 (2023) 121242.
42 Roesky P W, *Coord Chem Rev,* 206–207 (2000) 213
43 Banik H, Sarkar S, Bhattacharjee D, Malhotra A, Chauhan A & Hussain S A, *ACS Omega*, 9 (2023) 618.
44 Rahman F Y, Deb R, Sarkar S, Banik H, Uddin M J, Chakraborty S, Bhattacharjee D & Hussain S A, *ACS Appl Electron Mater*, 5 (2023) 3685.
45 Banik H, Sarkar S, Bhattacharjee D & Hussain S A, *ACS Appl Electron Mater*, 3 (2021) 5248
46 Deb R, Rahman F Y, Sarkar S, Banik H, Paul P K, Bhattacharjee D, Alibrahim K, Alodhayb K N & Hussain S A, *ACS Appl Eng Mater*, 2 (2024) 1141.
47 Banik H, Sarkar S, Rahman F Y, Kalita H, Bhattacharjee D & Hussain S A, *Mater Today Proc*, 65 (2022) 2773.
48 Chen J, Zhao T, He F, Zhong Y, Wang S, Tang Z, Qiu Y, Wu Z & Fang M, *Eur J Med Chem*, 254 (2023) 115341.